NASA/TM—2004-213226 AIAA–2004–3467

High Power MPD Thruster Performance Measurements

Michael R. LaPointe
Ohio Aerospace Institute, Brook Park, Ohio

Eugene Strzempkowski and Eric Pencil
Glenn Research Center, Cleveland, Ohio

September 2004

The NASA STI Program Office . . . in Profile

Since its founding, NASA has been dedicated to the advancement of aeronautics and space science. The NASA Scientific and Technical Information (STI) Program Office plays a key part in helping NASA maintain this important role.

The NASA STI Program Office is operated by Langley Research Center, the Lead Center for NASA's scientific and technical information. The NASA STI Program Office provides access to the NASA STI Database, the largest collection of aeronautical and space science STI in the world. The Program Office is also NASA's institutional mechanism for disseminating the results of its research and development activities. These results are published by NASA in the NASA STI Report Series, which includes the following report types:

- TECHNICAL PUBLICATION. Reports of completed research or a major significant phase of research that present the results of NASA programs and include extensive data or theoretical analysis. Includes compilations of significant scientific and technical data and information deemed to be of continuing reference value. NASA's counterpart of peer-reviewed formal professional papers but has less stringent limitations on manuscript length and extent of graphic presentations.

- TECHNICAL MEMORANDUM. Scientific and technical findings that are preliminary or of specialized interest, e.g., quick release reports, working papers, and bibliographies that contain minimal annotation. Does not contain extensive analysis.

- CONTRACTOR REPORT. Scientific and technical findings by NASA-sponsored contractors and grantees.

- CONFERENCE PUBLICATION. Collected papers from scientific and technical conferences, symposia, seminars, or other meetings sponsored or cosponsored by NASA.

- SPECIAL PUBLICATION. Scientific, technical, or historical information from NASA programs, projects, and missions, often concerned with subjects having substantial public interest.

- TECHNICAL TRANSLATION. English-language translations of foreign scientific and technical material pertinent to NASA's mission.

Specialized services that complement the STI Program Office's diverse offerings include creating custom thesauri, building customized databases, organizing and publishing research results . . . even providing videos.

For more information about the NASA STI Program Office, see the following:

- Access the NASA STI Program Home Page at ***http://www.sti.nasa.gov***

- E-mail your question via the Internet to help@sti.nasa.gov

- Fax your question to the NASA Access Help Desk at 301–621–0134

- Telephone the NASA Access Help Desk at 301–621–0390

- Write to:
  NASA Access Help Desk
  NASA Center for AeroSpace Information
  7121 Standard Drive
  Hanover, MD 21076

NASA/TM—2004-213226 AIAA–2004–3467

High Power MPD Thruster Performance Measurements

Michael R. LaPointe
Ohio Aerospace Institute, Brook Park, Ohio

Eugene Strzempkowski and Eric Pencil
Glenn Research Center, Cleveland, Ohio

Prepared for the
40th Joint Propulsion Conference and Exhibit
cosponsored by AIAA, ASME, SAE, and ASEE
Fort Lauderdale, Florida, July 11–14, 2004

National Aeronautics and
Space Administration

Glenn Research Center

September 2004

Acknowledgments

The following individuals provided expert engineering support and hardware fabrication during the performance of this research effort: Joseph Dick, James Coy, Donna Neville, Dennis Rogers, George Readus, George Rodriguez, and Ken Beno. The authors thank James Gilland and Pavlos Mikellides for several useful technical discussions.

This report contains preliminary findings, subject to revision as analysis proceeds.

Available from

NASA Center for Aerospace Information
7121 Standard Drive
Hanover, MD 21076

National Technical Information Service
5285 Port Royal Road
Springfield, VA 22100

Available electronically at http://gltrs.grc.nasa.gov

High Power MPD Thruster Performance Measurements

Michael R. LaPointe
Ohio Aerospace Institute
Brook Park, Ohio 44142

Eugene Strzempkowski and Eric Pencil
National Aeronautics and Space Administration
Glenn Research Center
Cleveland, Ohio 44135

High power magnetoplasmadynamic (MPD) thrusters are being developed as cost effective propulsion systems for cargo transport to lunar and Mars bases, crewed missions to Mars and the outer planets, and robotic deep space exploration missions. Electromagnetic MPD thrusters have demonstrated, at the laboratory level, the ability to process megawatts of electrical power while providing significantly higher thrust densities than electrostatic electric propulsion systems. The ability to generate higher thrust densities permits a reduction in the number of thrusters required to perform a given mission, and alleviates the system complexity associated with multiple thruster arrays. The specific impulse of an MPD thruster can be optimized to meet given mission requirements, from a few thousand seconds with heavier gas propellants up to 10,000 seconds with hydrogen propellant. In support of programs envisioned by the NASA Office of Exploration Systems, Glenn Research Center is developing and testing quasi-steady MW-class MPD thrusters as a prelude to steady-state high power thruster tests. This paper provides an overview of the GRC high power pulsed thruster test facility, and presents preliminary performance data for a quasi-steady baseline MPD thruster geometry.

Nomenclature

b	=	thrust coefficient
B	=	magnetic field strength
g	=	acceleration due to gravity
I_{sp}	=	specific impulse
j	=	current density
J	=	thruster current
J_{ci}	=	critical ionization current
$\dot{m}$	=	mass flow rate
m_a	=	propellant ion mass
P	=	power
r_a	=	anode radius
r_c	=	cathode radius
T	=	thrust
u	=	plasma velocity
u_{ci}	=	critical ionization velocity
V	=	thruster voltage
α	=	thrust coefficient parameter
ε_i	=	first ionization potential
η	=	efficiency
ξ	=	self-field MPD thruster scaling parameter
σ	=	plasma conductivity

I. Introduction

FUTURE in-space propulsion requirements for the economical delivery of lunar and Mars cargo, outer planet rendezvous and sample return, and other bold new ventures in deep space robotic and piloted planetary exploration have rekindled national interest in the development and deployment of high power plasma propulsion systems. High power electric propulsion systems offer several potential advantages over chemical engines for each of these mission types,[1-3] and the NASA Glenn Research Center (GRC) is working to develop high power (MW-class) electromagnetic thruster technologies to meet these demanding propulsion requirements. Current high power thruster research at NASA GRC is focused on the magnetoplasmadynamic (MPD) thruster, and includes systems analysis,[4] numerical modeling,[7-10] and experimental thruster testing. This paper provides an overview of MPD thruster operation, describes the GRC high power propulsion test facility, and discusses the experimentally measured performance of a quasi-steady, MW-class baseline MPD thruster operated with argon propellant.

II. Magnetoplasmadynamic Thruster

In its basic form, the magnetoplasmadynamic (MPD) thruster consists of an outer anode surrounding a central cathode (Fig. 1). A high-current arc is struck between the anode and cathode, which ionizes and accelerates a gas propellant. In self-field thrusters, the azimuthal magnetic field produced by the current returning through the central cathode interacts with the radial discharge current flowing through the plasma to produce an axial Lorentz body force, giving rise to the alternate Lorentz Force Accelerator (LFA) nomenclature often encountered in the literature. In applied-field versions of the thruster, a solenoid magnet surrounding the anode provides additional radial and axial magnetic fields that can help stabilize and accelerate the plasma discharge.

Initially investigated in the 1960's and funded periodically over the intervening decades, MPD thrusters have achieved slow but steady improvements in performance. For a detailed history of MPD thruster development, the reader is referred to a number of review papers that chronicle the progress and challenge of this promising in-space propulsion technology.[11-13] A variety of thruster geometries have been operated using different propellants, with lithium vapor propellant providing the most efficient performance to date. Lithium-fed MPD thrusters developed by the Moscow Aviation Institute in Russia have reported efficiencies of around 45%, with specific impulse (I_{sp}) values approaching 5000 s at power levels exceeding 100-kW.[14-18] Facilities to investigate lithium-fed MPD thrusters have been established in the United States at the Jet Propulsion Laboratory and Princeton University, with experimental results soon to be forthcoming.

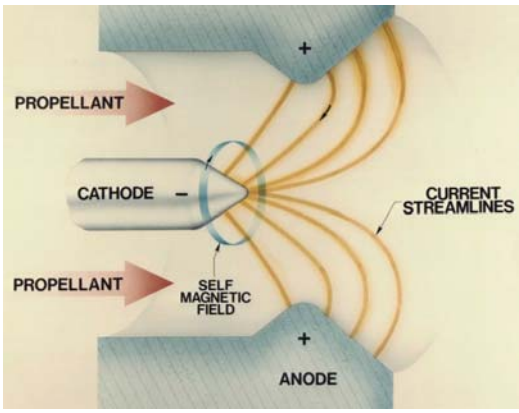

Figure 1. MPD thruster diagram.

While attractive from an efficiency viewpoint, a possible issue with lithium is that it is a condensable propellant with the potential to coat instrument surfaces and power arrays. In addition, the maximum achievable specific impulse with lithium is around 7500 s, while future power-rich robotic and piloted outer planet missions will require specific impulse values approaching 10000 s. These higher I_{sp} values may be achieved with hydrogen. As such, thrusters operating with non-condensable propellants are also being developed at various research facilities to better understand and improve gas-fed thruster performance.[19-25] Although gas-fed MPD thruster efficiencies have typically been lower than devices operated with lithium,[12,13,26] recent numerical models indicate that significantly improved performance can be achieved through the use of modified electrode geometries and the proper application of expansion nozzles and/or applied magnetic fields.[7,27,28] The use of non-condensable gas propellants mitigates possible ground handling and spacecraft contamination issues associated with lithium propellant, and may provide efficient thruster performance over a wide range of operating conditions. The NASA GRC effort is focused on the development and refinement of these high power gas-fed thruster technologies.

III. Pulsed MPD Thruster Test Facility

The pulsed, high power plasma thruster test facility at the Glenn Research Center consists of a high-energy pulse-forming network, interlocked vacuum chamber, propellant plenum, flexure-based thrust stand, and automated control systems. Following several design iterations, the facility became fully operational in late 2003 and has been used to investigate the performance of a baseline MPD thruster. The facility provides an economical test bed that can be used to characterize and improve the performance of prototype thruster geometries prior to undertaking more

expensive steady-state performance trials. The following sections provide a brief description of each of the major facility elements.

A. Pulse Forming Network

The pulse-forming network used for quasi-steady MPD thruster testing consists of 46 capacitors and 7 inductors arranged in a 7-element Guillemin network. Each capacitor is rated for 10-kVDC, with an expected shot life of 10^4 discharges at maximum charge voltage. The total bank capacitance is 4.88-mF, providing a maximum stored energy of 250-kJ at full charge. Switching is performed by a stack of solid-state thyristors rated for 15-kV and 50-kA peak current. Six of the inductors consist of insulated 0.95 cm (3/8") OD copper tubing wound around short sections of 27.3 cm (10.75") OD pvc pipe; the seventh inductor, which channels most of the discharge current, is constructed of insulated 2-AWG stranded cable. A 0.12-Ω matching resistor, rated for 10-kV and 250-kJ, is located in series between the switch and load. The capacitor bank and PFN are isolated from ground during each discharge. A 1000-Ω resistor rated for 250-kJ is tied into the bank via a relay switch and can be used to discharge the capacitors in the event of a thruster malfunction or safety interlock violation. The physical dimensions of the capacitor bank are 4.5 m (15 ft) long by 2.1 m (7 ft) high by 0.9 m (3 ft) wide. The total discharge period is approximately 2×10^{-3} s, with less than 10% current ripple over the discharge plateau.

B. Vacuum Chamber and Propellant Plenum

Pulsed MPD thruster tests are conducted in NASA GRC Vacuum Facility 1 (VF1). The vacuum chamber, shown in Fig. 2, is 1.5-m (5 ft) in diameter by 4.5-m (15 ft) long. Access to the chamber interior is provided through an endcap mounted on a balanced swing-arm. The tank is pumped by two 0.8-m (32") diameter oil diffusion pumps and a mechanical roughing pump, and is capable of reaching an unloaded base pressure of 10^{-6} torr (8×10^{-9} Pa). The vacuum tank is located on the floor above the capacitor bank, and power is cabled to the tank through high voltage feedthroughs located on a 1-m (36") bottom flange. Instrumentation and gas feedthroughs are located on a 0.4-m (16") side port, with additional access available through several 0.11-m (4.5") ports mounted to the facility endcap. A separate 0.4-m side port provides power cable access for a magnetic field coil, described in a later section of the paper.

Figure 2: High power vacuum facility VF-1.

The propellant gas plenum is mounted to a test cart located beside VF1 (Fig. 2). The cylindrical plenum chamber is constructed of stainless steel, with an interior volume of 2.5×10^{-2} m^3 (1.5×10^3 in^3). Stainless steel tubing connects one end of the plenum to a regulated gas bottle, while the other end is connected to a pneumatic actuator powered by a fast acting solenoid valve. Gas flow from the actuator can be directed either to the thruster through a side flange located in VF-1, or to a small calibration chamber located on the test cart. Short sections of the propellant feed line are constricted to a nominal inner diameter of 1.6-mm (1/16") both upstream of the thruster and upstream of the calibration chamber, to ensure choked flow conditions are achieved along each propellant flow path. The stainless steel calibration chamber has an internal cylindrical volume of 6.1×10^{-3} m^3 (3.7×10^2 in^3) and is used to measure the amount of gas discharged during pulsed operation. Both the propellant plenum and the calibration chamber are outfitted with wide-ranging pressure gauges (dual pirani gauge and diaphragm manometer), capable of measuring pressure values from 10^{-3} torr to 1800 torr (0.13-Pa to 2.4×10^5-Pa).

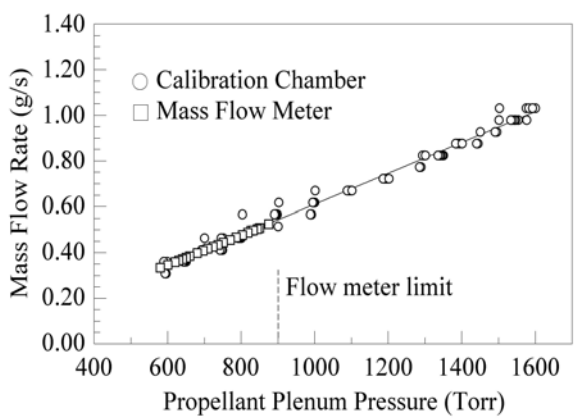

Figure 3: Argon mass flow calibration.

During calibration, the propellant plenum pressure is set to a given value, and the calibration chamber is evacuated to vacuum. Gas from the propellant plenum is discharged into

the calibration plenum, and the resulting pressure rise is recorded. Knowing the pressure change and the chamber volume allows the propellant mass injected into the calibration chamber to be calculated, and dividing this mass by the total response period of the pneumatic actuator provides the propellant flow rate for the pulsed discharge (Fig. 3). The flow period of the actuator can be set between 140-ms and 230-ms through the use of a variable resistor in the control circuit; a value of 180-ms is currently used to ensure the gas flow reaches the thruster and to reduce uncertainties in the actuator opening and closing response times. The plenum is presently rated for a pressure of approximately 1520-torr (2-atm), limiting the maximum argon mass flow rate to around 1.0-g/s.

As a second check on mass flow calibration, a fast-acting mass flow meter has recently been installed in the propellant feed line. The propellant plenum is set to a given pressure, and an electrical switch is used to open the actuator valve for a period of approximately 1-second, with propellant flow directed to the evacuated calibration chamber. Mass flow rates in units of sccm are measured and displayed by the mass flow meter, with values subsequently converted to mass flow rate in grams per second. As shown in Fig. 3, the results of this independent calibration of mass flow rate are in excellent agreement with the linear curve fit to the volumetric flow rate calibrations, up to the measurement limit of the flow meter. Based on the combined flow meter data and the independently obtained calibration curve obtained with the calibration chamber technique, the mass flow rate is estimated to have an uncertainty of less than +/- 5%.

C. Thrust Stand

The pulsed MPD thrust stand is based on a simple flexure design (Fig. 4). The thruster is mounted to a stiff horizontal plate, which in turn is supported by four thin, contoured aluminum flexures mounted to a bottom support plate. Current is fed to the thruster through high voltage coaxial cables, with return currents traveling through the cable shields to reduce magnetic tare forces on the thrust stand. During discharge, the upper plate of the thrust stand is horizontally displaced by the thruster impulse. A calibrated dynamic load cell is used to measure the resulting impulse, and the time-dependent load cell response is measured using an oscilloscope. The load cell is mounted to a vertical support hanging from the moveable upper plate of the thrust stand, and a ceramic magnet is mounted to the face of the load cell. A vacuum rated linear actuator is mounted to a vertical support column on the fixed bottom plate of the thrust stand, in line with the load cell, and a separate ceramic magnet of like polarity is mounted to the actuator tip. The repulsive magnetic fields between the magnets provides a firm coupling between actuator and load cell, while the lack of actual physical contact minimizes the facility background noise transmitted to the load cell. A consistent magnetic coupling force is achieved prior to each thruster test sequence (or thrust stand calibration) by a preprogrammed movement of the actuator to produce a predetermined peak load cell response.

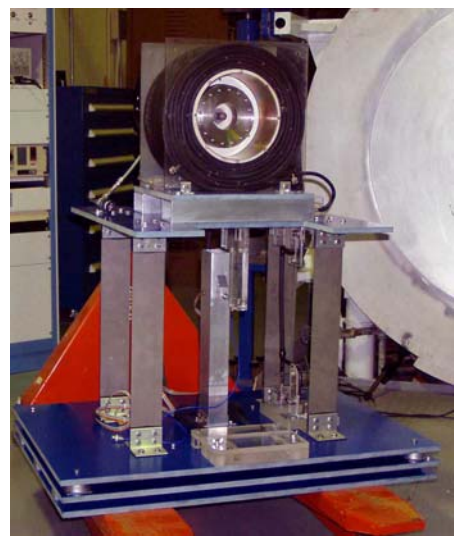

Figure 4. MPD thrust stand.

The thrust stand is calibrated outside the vacuum chamber using a fixed-mount electronic impact hammer; the hammer tip impacts a separate dynamic load cell mounted on a stiff plate spanning the face of the thruster anode, and the resulting impulse (time-integrated response) is measured by the load cell on the thrust stand. The total impulse delivered by the impact hammer, as measured by the impact load cell, is correlated to the total impulse of the thrust stand response, as measured by the thrust stand load cell. The resulting measurements provide a calibration curve that can be used to determine thruster impulse based on integrated load cell response (Fig. 5). Integrated thrust stand impulse measurements obtained during impact hammer testing typically fall within +/-10% of the calibration

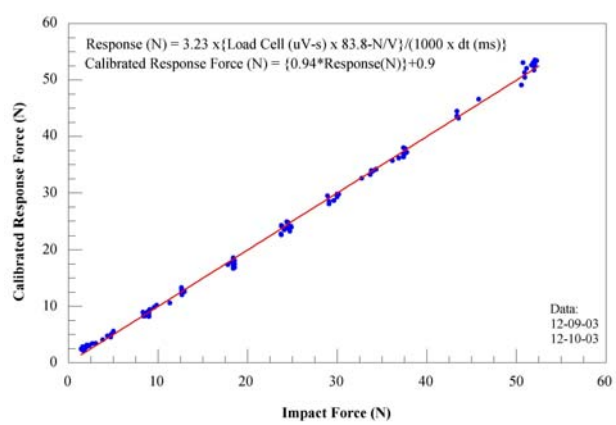

Figure 5: Thrust stand calibration curve.

curve for impact forces exceeding approximately 4-N; below this value the stiffness of the stand produces less reliable results.

The present thrust stand configuration does not allow in-situ calibration under vacuum conditions; however, a solid-state inclinometer mounted beneath the top plate of the thrust stand is used to provide information on the initial and final orientation (2-axis tilt) of the stand. No significant differences have been observed between thrust stand orientations at rest in air or under vacuum, assuring that the measured impulse values will closely correspond to the calibrated thrust stand values.

D. Applied Field Magnet

Prior research has shown that it may be advantageous to operate MPD thrusters with axial and radial magnetic fields provided by external solenoid magnets.[12,13,27,28] Although not used in the self-field performance data reported below, this option is available through the use of an un-cooled magnet consisting of insulated 4-AWG copper cabling wound on a 0.2-m (8") OD pvc pipe. The insulated cabling is continuously wound in 7 layers, with 18 turns per layer. Because the magnet is not cooled, both the maximum current and the period of operation are limited; however, the simplicity of operation and the field strength achieved over the short thruster pulse period outweigh these disadvantages. Power is supplied by a 50-kW constant-current arc welder, capable of delivering up to 1000 A to the magnet. The measured axial magnetic field strength at the center of the magnet coil is roughly 5×10^{-4} Tesla/Amp, while at the end of the coil the axial field along the centerline is approximately 3.3×10^{-4} Tesla/Amp.

E. Control Systems

The events leading up to a pulsed thruster discharge are controlled with an automated sequencing system mounted in the MPD control rack. If the applied-field magnet is to be used, the magnet power supply is preset to the desired current level. The capacitor bank is then charged to the desired voltage using a 4-kW, 10-kV power supply located in the control rack. Once the bank is charged to the desired voltage, the charging supply is disengaged and the test sequence is initiated. For applied-field operation, the magnet power is turned on and operates for a period of 4.5 s, sufficient to establish a constant field distribution within the thruster and to allow any residual thrust stand disturbances due to switching on the magnet to damp away. At the end of this period, a timer activates the propellant plenum solenoid to provide gas flow to the thruster; as noted, the duration of the gas pulse can be set from approximately 140-ms to 230-ms, with the present value set to 180-ms to ensure proper gas flow to the thruster. The capacitor bank switch is triggered at the end of the gas pulse timer, providing an approximately 2-ms, high current discharge to the thruster. Once the bank has fired, the control sequence turns off the gas flow, waits approximately 500 milliseconds and turns off the magnet current (to prevent magnet tare forces from interfering with thruster data collection), and then the logic system automatically resets to initiate another test sequence.

F. Data Collection

The primary diagnostics at this stage of facility development include thruster voltage and current, thrust stand displacement, and magnet coil temperature. Thruster voltage and current are used to calculate the thruster power. Voltage, current, thrust, and mass flow rate are combined to determine thruster efficiency, η:

$$\eta = \frac{T^2}{2\dot{m}VJ} \tag{1}$$

where T is the thrust (N), $\dot{m}$ is the propellant mass flow rate (kg/s), V is the discharge voltage, and J is the thruster operating current.

Digital oscilloscopes measure and record the thruster voltage, thruster current, and load cell voltage waveforms, which are then transferred to a desktop computer for later analysis. Differential voltages are measured across the thruster electrodes using a voltage attenuation (resistor network) circuit to scale the voltage channels and prevent waveform clipping by the oscilloscopes. The differential voltage is measured over a 500-μs period in a quiescent portion of the 2-ms discharge, with a typical uncertainty of ± 5%. Two independent current monitors (transformers) are used to record the pulsed current into and out of the thruster. The coils are rated for 50-kA peak current, a current-time product of 65 A-s, and a rise time of 2.5×10^{-7} s. The discharge current is measured over the same 500-μs period as the differential voltage; due to slight oscillations in the current waveform, the measurement uncertainty in the discharge current is approximately ±5%.

The temperature of the thruster is not expected to increase significantly during each 2-ms discharge, and the period between pulses is sufficiently long (on the order of several minutes) that thruster electrode temperature measurements are not required. However, the coil current will resistively heat the magnet during the few seconds of

operation required for applied-field MPD thruster tests, hence thermocouples have been embedded in the coil to monitor the temperature rise and to signal when testing should be suspended to allow the magnet to cool.

G. Baseline MPD Thruster Geometry

Based on numerical simulations using a GRC MPD thruster code,[5,6] a laboratory-model MPD thruster was designed and fabricated and is presently undergoing performance testing in self-field mode over power ranges from a few hundred kilowatts up to a few megawatts. Shown in Fig. 6, the GRC baseline thruster employs an anode lip, similar in design to the Princeton University benchmark MPD thruster.[26] The un-cooled baseline thruster anode is constructed of stainless steel, with disks bolted together to form the anode chamber and the constricted lip region. The chamber depth is approximately 5.2 cm from backplate to anode face, with an internal chamber radius of 5.7 cm. The anode lip differs somewhat from the Princeton benchmark design, with the current lip geometry set at 3.8 cm long and 2.5 cm deep. A 0.95-cm radius tungsten rod cathode extends approximately 4.8-cm from the backplate, ending in a 45° conical tip. The electrically insulating backplate separating the anode and cathode is composed of boron nitride. A propellant injection ring with a mean radius of 4-cm fits within a circular groove in the boron nitride; propellant enters the thruster through ten evenly spaced holes, each 1/16" (0.15 cm) in diameter, drilled in the downstream face of the ring. The thruster assembly is mounted within the solenoid magnet (Fig. 7), and the whole assembly is bolted to the top plate of the thrust stand.

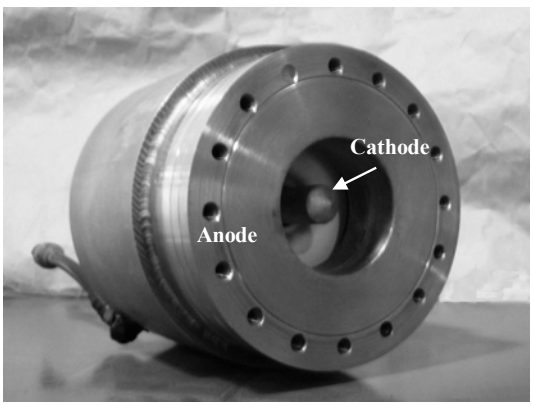

Figure 6: Baseline MPD thruster.

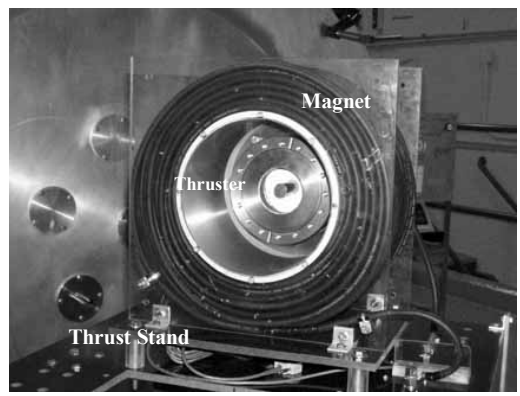

Figure 7: Thruster mounted on thrust stand.

IV. Baseline Thruster Test Results

The baseline MPD thruster was tested at three mass flow rates (0.25-g/s, 0.5-g/s, and 0.75-g/s) over a range of discharge currents up to the current level at which significant terminal voltage oscillations were observed. This unsteady operating condition, typically termed "onset" in the MPD literature, corresponds to a significant increase in electrode erosion and sets an upper limit on the current at which a thruster can be operated for a given mass flow rate. Present theories on the cause of onset in MPD thruster center on the depletion of charge carriers in the anode region as the current is increased above a critical value, resulting in a transition from diffuse arc attachment to spot mode attachment at the anode.[29]

Choueiri[30,31] developed a self-field MPD thruster scaling parameter, ξ, which relates the discharge current J to a critical current J_{ci} at which full propellant ionization is expected to occur:

$$\xi = J / J_{ci} \tag{2}$$

The critical ionization current is a function of the propellant mass flow rate, critical ionization velocity, and thruster geometry:

$$J_{ci} = \left[\frac{\dot{m} u_{ci}}{b} \right]^{1/2} \tag{3}$$

where u_{ci} is the critical ionization velocity,

$$u_{ci} = \left(\frac{2\varepsilon_i}{m_a}\right)^{1/2} \tag{4}$$

and b is a coefficient that takes into account thruster geometry:

$$b = \frac{\mu_0}{4\pi}\left[\ln\left(\frac{r_a}{r_c}\right) + \alpha\right] \tag{5}$$

In Equation 5, r_a is the anode radius, r_c is the cathode radius, and α is a parameter (0< α <1) which depends on the details of the current attachment to the electrodes.[32] For the baseline thruster operating with argon propellant, the critical ionization velocity is 8,720 m/s. The anode to cathode radius is 6.0 using the larger anode radius of 5.7 cm, and 3.4 using the anode lip radius of 3.2 cm. The actual value of the thrust coefficient for the self-field baseline MPD thruster is determined from the experimental data presented below. Stable operation of self-field MPD thrusters is observed to occur for values of $\xi \leq 2$; higher currents lead to the onset of instabilities which are manifested by unstable terminal voltages, spot mode current attachment to the anode, and increased electrode erosion leading to reduced thruster lifetime.

A. Current-Voltage Measurements

Figure 8 displays current and voltage waveforms for the baseline thruster operated at an argon mass flow rate of 0.5-g/s and a discharge current of 7.4-kA (ξ=1.5). The voltage and current values are measured over the last 500-μs of the approximately 2-ms discharge, to more accurately represent quasi-steady thruster performance. The discharge current and differential voltage waveforms are steady over the measurement period, indicating the thruster is operating below onset. Increasing the discharge current while holding the mass flow rate constant eventually leads to a condition where significant hash is recorded on the voltage waveform, heralding the onset of unstable thruster operation. The level of voltage hash typically used to demark thruster operation at onset is 10% of the voltage signal. Figure 9 displays the current and voltage waveform for the baseline thruster operated at an argon mass flow rate of 0.5-g/s and a discharge current of 14.5-kA (ξ=2.9). The hash in the voltage waveform is readily apparent, indicating the thruster is operating above onset at this discharge current. If the thruster were to operate in steady-state at this operating condition, the electrodes would suffer significant erosion due to spot-mode attachment of the current, leading to substantially shortened thruster lifetime.

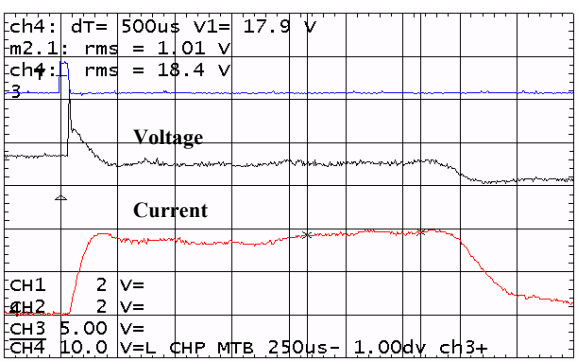

Figure 8. Voltage (V) and current (J) waveforms for baseline MPD thruster, 0.5-g/s argon, operating below onset. V=112-V, J=7.4-kA.

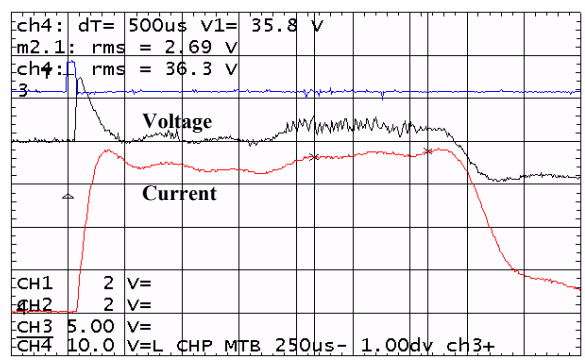

Figure 9. Voltage (V) and current (J) waveforms for baseline MPD thruster, 0.5-g/s argon, operating above onset. V=290-V, J=14.5-kA.

Figure 10 below displays voltage-current curves for the self-field baseline MPD thruster for the three argon mass flow rates investigated. Also shown in the figure are the discharge currents at which onset is experimentally observed to occur. Error bars have been suppressed for clarity; typical errors in voltage measurements are +/-5% of the measured value (see Section III-F). Table 1 lists the experimentally observed current at which onset occurs for each mass flow rate, and the corresponding value of the thruster scaling parameter $J^2/\dot{m}$.

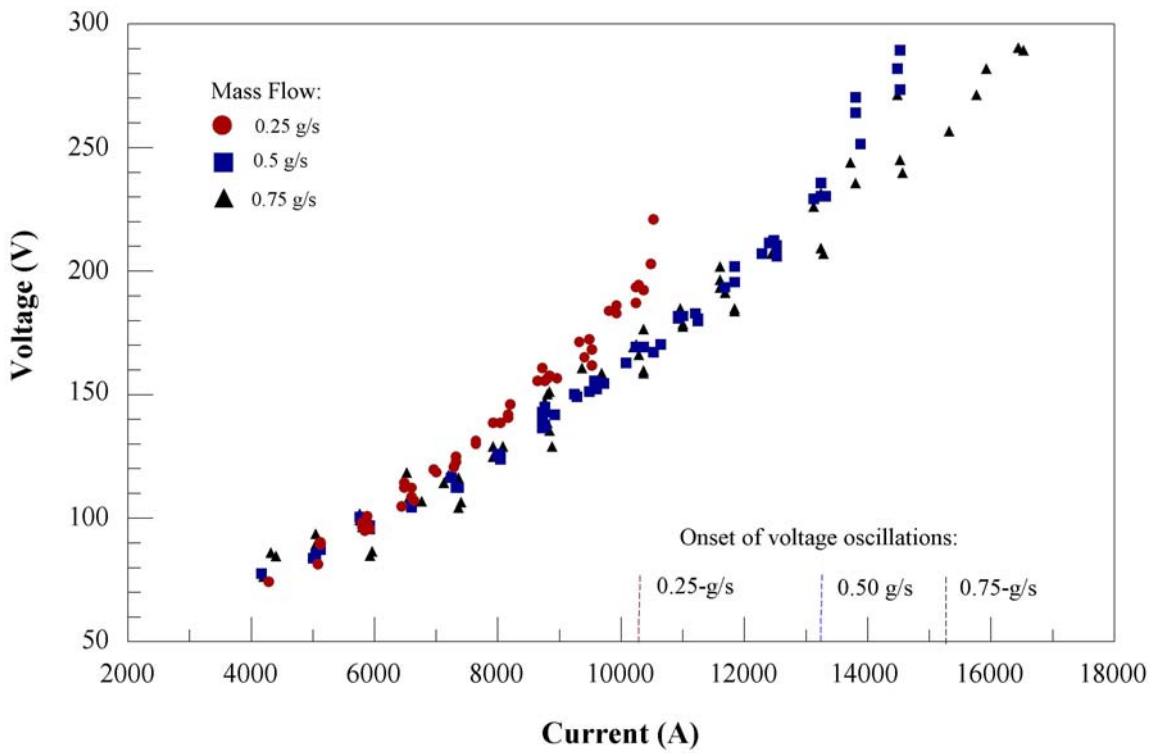

Figure 10. Voltage-current curves for self-field baseline MPD thruster operated with argon propellant, including experimentally determined values of onset current. Error bars suppressed; voltage values +/- 5%.

Table 1. Experimentally measured current at which the onset of voltage instabilities occurs and corresponding values of $J^2/\dot{m}$

Mass Flow Rate (g/s)	**Onset Current (kA)**	$J^2/\dot{m}$ (kA^2-s/g)
0.25	10.2	416
0.50	13.2	350
0.75	15.2	308

As expected from prior MPD thruster experiments and theoretical analysis, the thruster operating voltage is generally higher at a given discharge current for lower mass flow rates, and deviates from a linear Ohm's-law relation at higher discharge currents.[26,32,33] The terminal voltage can be modeled as:[33]

$$V = \int \frac{\vec{j}}{\sigma} \cdot d\vec{l} + \int \left(\vec{u} \times \vec{B}\right) \cdot d\vec{l} + V_F \tag{6}$$

where j is the current density, σ is the plasma conductivity, u is the plasma velocity, B is magnetic field strength, and V_F is an electrode fall potential that incorporates sheath potentials and electrode heating. Integrating the first term over a path length *dl* between the electrodes yields a linear Ohm's law between voltage and current; integrating the second term and assuming electromagnetic thrust (proportional to bJ^2) as the dominant component yields a term proportional to the cube of the current and inversely proportional to mass flow rate:

$$V \sim b^2 J^3 / \dot{m} \tag{7}$$

At higher discharge currents this voltage term is expected to dominate the linear ohm term. Both the inverse dependence on mass flow rate and the nonlinear increase in voltage are observed in the voltage traces displayed in Figure 10, becoming more pronounced as the thruster approaches operation at or above the onset condition.

B. Thrust Measurements

Figure 11a displays the thrust stand response corresponding to the thruster operating condition shown in Figure 8 ($\dot{m}$=05-g/s, J=7.4-kA), while Figure 11b shows the thrust stand response for a cold gas discharge taken at the same mass flow rate immediately after the thruster test. Background noise levels were the same for each shot.

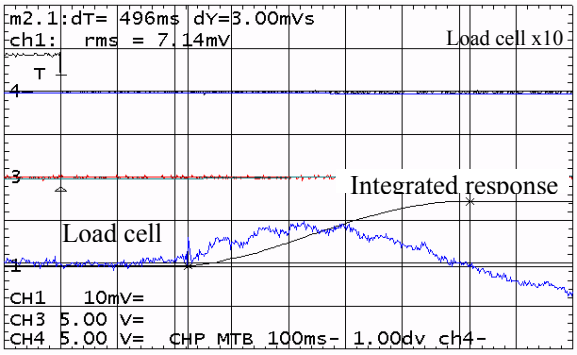

Figure 11a. Load cell measurement of thrust stand response for baseline thruster operated at 0.5-g/s (argon) at a discharge current of 7.4-kA.

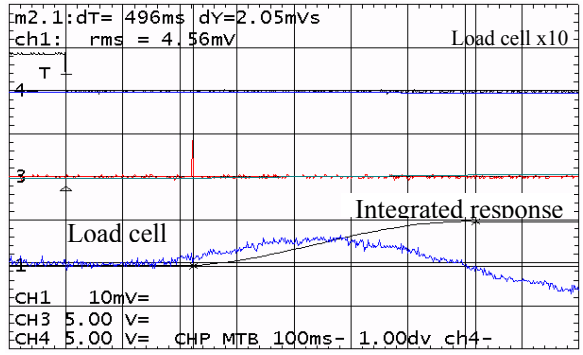

Figure 11b. Load cell measurement of thrust stand response for baseline thruster operated with cold gas discharge at 0.5-g/s (argon).

To determine the impulse delivered to the thrust stand by the thruster discharge, the time-integrated response of the thrust stand to the cold gas discharge (0.205-mVs) is subtracted from the time-integrated response of the stand to the combined cold gas flow and thruster discharge (0.300-mVs). Because the cold gas flow occurs over a period of approximately 200-ms, while the thruster discharge occurs for approximately 2-ms, the subtraction of the cold gas value from the total impulse value provides an accurate measure of the thrust stand response to the thruster discharge. Actually, the subtraction of the 200-ms cold gas impulse from the total impulse slightly underestimates the thruster impulse by neglecting the contribution of the cold gas during the 2-ms discharge; however, neglecting the contribution of the miniscule 2-ms worth of cold gas impulse does not produce significant errors in the final thrust value. Using the impact hammer calibrations to convert the net impulse to a force value yields a thrust of approximately 13.5-N for the baseline thruster operating at this mass flow and current level.

Figure 12 displays thrust measurements for the self-field baseline thruster corresponding to the range of mass flow rates and discharge currents shown in Figure 10. As in that figure, the discharge currents where onset was experimentally determined to occur are also shown in Figure 12. Error bars are again suppressed for clarity; typical uncertainties in the measured thrust are +/-10% for force values above 4-N; below this value the thrust stand is too stiff for accurate force measurements to be obtained.

Also shown in Figure 12 is a plot of the electromagnetic thrust expected from the Maecker formula, given by:[32]

$$T_{EM} = bJ^2 \tag{8}$$

where J is the discharge current and b is the thrust coefficient, which was determined from the experimental data by plotting the value of T/J^2 as a function of current, as shown in Figure 13. For higher values of current, the curves for the three mass flow rates collapse onto a single line yielding a value of $b=1.8\times10^{-7}$ N/A^2; this value was used in Eqn. 8 to produce the curve shown in Figure 12.

Equation 8 accurately predicts the thrust values at higher discharge currents, but underpredicts the thrust at lower discharge currents. Prior analyses of MPD thruster experiments have typically attributed this discrepancy to the larger fractional contribution of ohmically heated gas at lower currents; however, recent analysis by Choueiri indicates that the departure may instead result from pressure distributions created by the pinching components of the volumetric electromagnetic body forces.[30,31] As discussed by Choueiri and more recently by Gilland,[32] Eqn, 8 is expected to hold for higher discharge currents where the electromagnetic thrust is the dominant contributor; however, the formula must modified for currents below the critical ionization current (ξ<1):

$$T = \begin{matrix} \dot{m}u_{ci}\xi & (\xi < 1) \\ bJ^2 & (\xi > 1) \end{matrix} \tag{9}$$

Given a critical ionization velocity for argon of 8720 m/s and a thrust coefficient of 1.8×10^{-7} N/A^2, the critical ionization currents for the various mass flow rates used in the experiments are 3480 A, 4920 A, and 6025 A for mass flow rates of 0.25-g/s, 0.5-g/s, and 0.75-g/s, respectively. Using these values in Eqn. 9 yields reasonable thrust estimates for the higher 0.75-g/s flow rate, but significant discrepancies in predicted and measured thrust still occur for $\xi<1$ at the lower mass flow rates, indicating a discrepancy either in the formula or the thrust data at these very low mass flow rates and low currents. The Maecker formula does match the experimental data at each flow rate for values of $\xi>1$, and as expected the thrust is relatively independent of mass flow rate for these operating conditions.

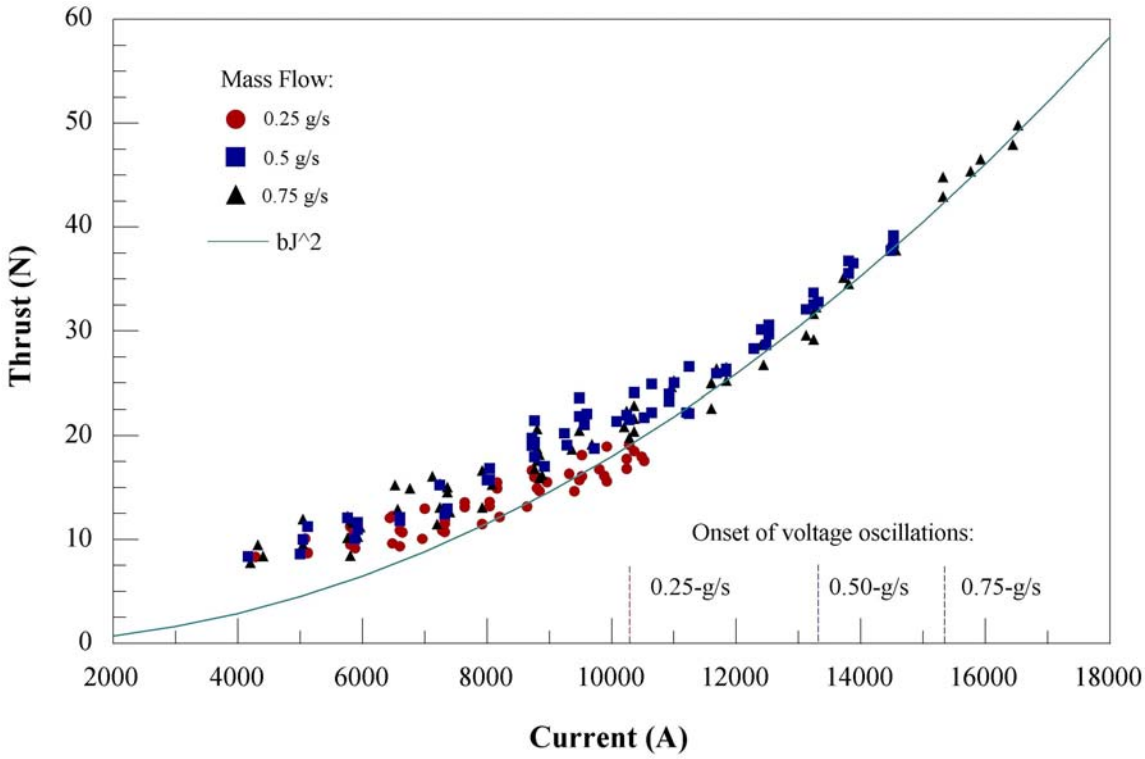

Figure 12. Thrust as a function of discharge current for the self-field baseline MPD thruster. Error bars suppressed; thrust values +/-10%.

Returning to Eqn.5, the value of α in the thrust coefficient can now be determined. Using an anode radius of 5.7-cm and cathode radius of 0.95-cm, the value of b with α=0 is approximately 1.8×10^{-7} N/A^2, which would seem to closely agree with the experimentally determined value shown in Figure 13. However, examination of the thruster anode indicates that most of the current attachment occurs within the anode lip, corresponding to an anode radius of 3.2-cm. Using this value in Eqn. 5 and setting the value of b equal to the experimentally determined yields a value for α of approximately 0.6, within the mid-range of values typically found for this coefficient.

Finally, it is of interest to determine whether the value of the scaling parameter ξ can be correlated to the onset of instabilities in the GRC baseline thruster, as determined by Choueiri for other thruster geometries.[31,33]

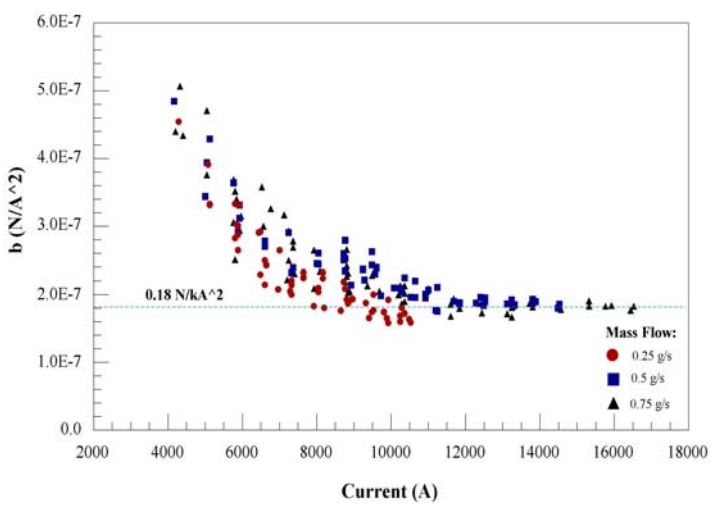

Figure 13. Experimentally determined thrust coefficient for the self-field baseline MPD thruster

These prior results indicate that stable thruster operation occurs for $\xi \leq 2$, with higher values leading to onset and increased electrode erosion. For the baseline thruster, the experimentally determined values of ξ for the critical ionization and onset currents listed above are 2.9, 2.7, and 2.5 for mass flow rates of 0.25-g/s, 0.5-g/s, and 0.75-g/s respectively. The experimentally determined values of ξ are somewhat higher than the expected value of $\xi \approx 2$ for onset, possibly due again to the significantly lower mass flow rates used in this study compared to those in the analysis by Choueiri. This is plausible, given that the trend in the onset data for the baseline thruster is toward $\xi = 2$ with increasing mass flow rate.

C. Efficiency Measurements

The efficiency of the baseline thruster at each mass flow rate can be calculated with Equation 1 using the experimentally measured values of thrust, current and voltage. Due to the uncertainty in mass flow rate (+/-5%), voltage (+/-5%), current (+/-5%), and thrust (+/-10% above 4-N, inaccurate below 4-N), the relative error in the efficiency calculations is +/-35% ($\Delta\eta/\eta$ = +/-0.35). Multiplying thruster current and voltage to obtain thruster power, the efficiency is displayed in Figure 14 as a function of power, again with error bars suppressed for clarity. Efficiency values for thruster operation at or above onset are not included in the figure. Although there is significant scatter in the efficiency estimates, particularly for the lower mass flow rates at lower power, the trend is toward increasing efficiency with increasing power, approaching 30% to 35% for each of the mass flow rates.

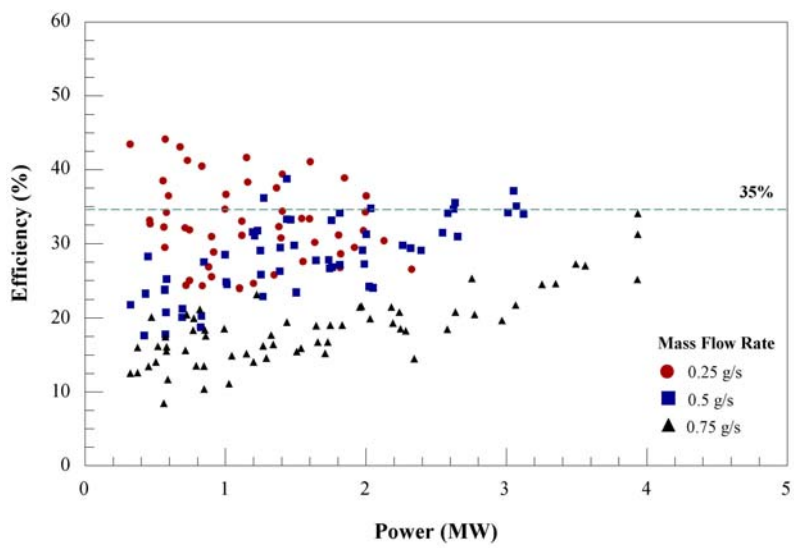

Figure 14. Baseline MPD thruster efficiency vs. power; data above onset not included. Error bars suppressed; $\Delta\eta/\eta$ = +/- 35%

D. Specific Impulse

Figure 15 plots the relation between specific impulse and discharge power for the baseline MPD thruster, where specific impulse, I_{sp}, is calculated using:

$$T = \dot{m} g I_{sp} \tag{10}$$

The relative error, ΔI_{sp}, in specific impulse calculations arising from the uncertainty in the thrust and mass flow measurements are +/-15% ($\Delta I_{sp}/I_{sp}$ = +/-0.15). As in prior figures the error bars have been suppressed for clarity, and the values of specific impulse obtained for thruster operation at or above onset are not included in the figure.

While once again there is significant scatter in the data, especially at the lower mass flow rates, the specific impulse varies inversely with mass flow rate (as expected from Eqn. 10) and increases approximately linearly with increasing power. The linear increase with power is a consequence of the relatively linear nature of the voltage-current relation observed for the baseline

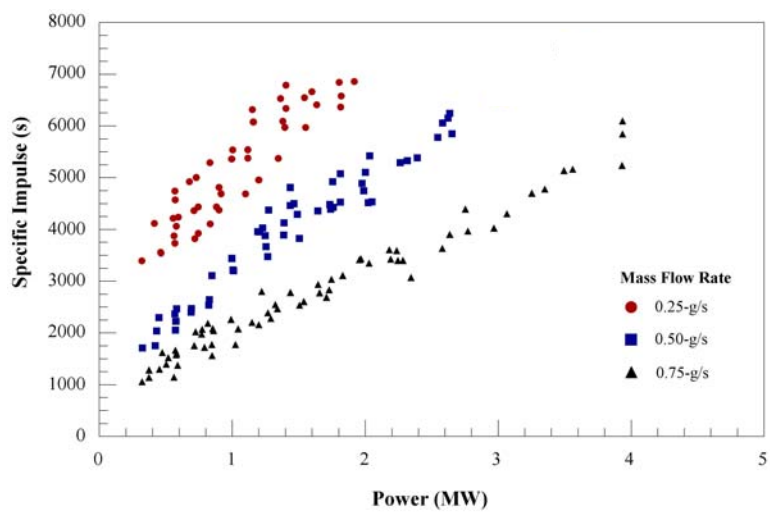

Figure 15. Baseline MPD thruster specific impulse vs. power; Error bars suppressed; $\Delta I_{sp}/I_{sp}$ = +/-15%.

thruster over most of the current range. The specific impulse is proportional to the thrust and increases with the square of the current, while the power is proportional to current and voltage. As noted in Figure 10, the voltage is nearly linear with increasing current over most of the current range until nearing the onset condition, after which a nonlinear rise in voltage is observed. Consequently the power scales as the square of the current over this same current range, resulting in the nearly linear I_{sp}-power curves occurring below onset. At higher discharge powers (where the voltage relationship is no longer linear) the I_{sp} curve will begin to flatten out with increasing power level, a relation hinted at but not readily apparent in the limited data sets shown in Figure 15.

For the self-field baseline thruster operating with an argon mass flow rate of 0.25-g/s, the specific impulse reaches a value of nearly 7000 s before the occurrence of onset. At 0.5-g/s, the maximum specific impulse is approximately 6300 s, while at 0.75-g/s the maximum specific impulse before onset is around 6000 s. These I_{sp} values are substantially higher than prior experimental data obtained with other self-field MPD thruster geometries operated with argon propellant,[12,13,26] and should be repeated to confirm their validity.

V. Concluding Remarks

A facility to test high power MPD thrusters has been established at the NASA Glenn Research Center, and is currently being used to evaluate the quasi-steady performance of a baseline MPD thruster geometry at power levels from 500-kW to several megawatts. Preliminary test results have been obtained with argon propellant over a range of mass flow rates, demonstrating self-field MPD thruster efficiencies approaching 35% with specific impulse values in excess of 6000 s prior to the measured onset of thruster instabilities. If verified by further testing, this combination of specific impulse and efficiency exceeds the performance of prior self-field MPD thruster geometries operated with argon propellant. Even still, the efficiency of the MPD thruster must be improved to make it competitive with other near-term in-space propulsion options. Toward this end, operation of the baseline MPD thruster with hydrogen propellant and with applied magnetic fields will be undertaken in the near future. Prior analysis has shown that the proper application of axial and radial magnetic fields can increase thermal contributions to the total thrust through viscous heating of the propellant gas, which is anticipated to result in an improvement in thruster efficiency.[27,28] Previous research at Princeton University demonstrated quasi-steady self-field thruster operation up to several megawatts with hydrogen propellant, reaching efficiencies of 50% and specific impulse values in excess of 10000 s. [26] Although preliminary, the results indicate efficient high power operation of MPD thrusters can be achieved at specific impulse values of interest for future deep space exploration missions.

In support of the thruster experiments, numerical modeling using in-house codes and advanced MACH2 simulatons[27] will be used to analyze and improve MPD thruster performance. Improved thruster designs based upon the numerical simulations will be tested in the pulsed GRC facility, with the goal of demonstrating gas-fed thruster efficiencies of at least 50%. Longer term efforts will focus on the refurbishment of a steady-state MPD thruster test facility at NASA GRC and possible research collaborations with the University of Stuttgart's plasma thruster test facility[34] to provide combined performance and lifetime measurements of high power gas-fed steady-state MPD thrusters.

References

[1]Gilland, J., "Mission and System Optimization of Nuclear Electric Propulsion Vehicles for Lunar and Mars Missions," NASA CR-189058, Dec. 1991.

[2]Filliben, J. D., "Electric Propulsion for Space Applications," Report CPTR96-64, Chemical Propulsion Information Agency, Columbia, MD, 1996.

[3]Oleson, S., "Advanced Electric Propulsion for Space Solar Power Satellites," NASA/TM-1999-209307, Aug. 1999.

[4]Gilland, J., "MPD Thruster Performance Models for System and Mission Analysis," AIAA-2003-4841, *39th AIAA/SAE/ASME/ASEE Joint Propulsion Conference*, Huntsville, AL, July 2003.

[5]LaPointe, M. R., "Numerical Simulation of Geometric Scale Effects in Cylindrical Self-Field MPD Thrusters," AIAA-92-3297, *28th AIAA/SAE/ASME/ASEE Joint Propulsion Conference*, Nashville, TN, July 1992.

[6]LaPointe, M. R., "Numerical Simulation of Cylindrical, Self-Field MPD Thrusters with Multiple Propellants," NASA CR-194458, Jan. 1994.

[7]LaPointe, M. R. and Mikellides, G., "Design and Operation of MW-Class MPD Thrusters at the NASA Glenn Research Center," AIAA-2002-4133, *38th AIAA/SAE/ASME/ASEE Joint Propulsion Conference*, Indianapolis, IN, July 2002.

[8]Mikellides, P. G., "Theoretical Investigation of Magnetoplasmadynamic Thrusters," Ph.D. Dissertation, Department of Aeronautical and Astronautical Engineering, Ohio State University, 1994.

[9]Mikellides, P. G. and Turchi, P., "Application of the MACH2 Code to Magnetoplasmadynamic Arcjets", AIAA-92-3740, *28th AIAA/SAE/ASME/ASEE Joint Propulsion Conference*, Nashville, TN, July 1992.

[10]Sleziona, P. C>, Auweter-Kurtz,M., and Schrade, H. O., "Numerical Calculation on Nozzle-Type and Cylindrical MPD Thrusters", AIAA-92-3296, *28th AIAA/SAE/ASME/ASEE Joint Propulsion Conference*, Nashville, TN, July 1992.

[11]Nerheim, N. and Kelly, A., "A Critical Review of the Magnetoplasmadynamic Thruster for Space Applications," NASA CR-92139, Feb. 1968.

[12]Sovey, J. and Mantenieks, M., "Performance and Lifetime Assessment of Magnetoplasmadynamic Arc Thruster Technology," NASA TM-101293, 1988.

[13]Myers, R., Mantenieks, M., and LaPointe, M., "MPD Thruster Technology," NASA TM-105242, 1991.

[14]Tikhonov, V., Semenikhin, S., Brophy, J., and Polk, J., "Performance of 130-kW MPD Thruster with an External Applied Field and Lithium as Propellant," IEPC-97-120, *25th International Electric Propulsion Conference*, Cleveland, OH, 1997.

[15]Polk, J., Tikhonov, V., Semenikhim, S., and Kim, V., "Cathode Temperature Reduction by Addition of Barium in High Power Lithium Plasma Thrusters," in *Space Technology and Applications International Forum (STAIF) 2000*, edited by M. el-Genk, AIP Conference Proceedings 504, Melville, NY, 2000, pp. 1556-1563.

[16]Kodys, A., Cassady, L., and Choueiri, E., "Performance of a 30-kW Applied-Field Lithium Lorentz Force Accelerator,", AIAA-2003-4842, *39th AIAA/SAE/ASME/ASEE Joint Propulsion Conference*, Huntsville, AL, July 2003.

[17]Kodys, A., Emsellem, G., Cassady, L., Polk, J., and Choueiri, E., "Lithium Mass Flow Control for High Power Lorentz Force Accelerators," *Space Technology and Applications International Forum (STAIF) 2001*, edited by M. El-Genk, AIP Conference Proceedings 552, Melville, NY, 2001, pp. 908-915.

[18]Sankaran, K., Jardin, S. C., and Choueiri, E. Y., "Study of Plasma Flows in Lithium Lorentz Forced Accelerators Using Numerical Simulations," AIAA-2003-4843, *39th AIAA/SAE/ASME/ASEE Joint Propulsion Conference*, Huntsville, AL, July 2003.

[19]Toki, K. and Shimizu, Y., "Study of Low-Power MPD Propulsion for Future High-Power Trend," AIAA-2002-4115, *38th AIAA/ASME/SAE/ASEE Joint Propulsion Conference*, Indianapolis IN, July 2002.

[20]Kinefuchi, K., Toki, K., and Funaki, I., "Nozzle Shape Effects on Velocity Distribution in an MPD Arcjet," IEPC-2003-56, *28th International Electric Propulsion Conference*, Toulouse, France, Mar. 2003.

[21]Auweter-Kurtz, M., "Plasma Thruster Development Program at the IRS," *Acta Astronautica*, **32** (5), 1994, pp. 377-391.

[22]Auweter-Kurtz, M., Epple, J., Habiger, H., Kurtz, H., Loesener, O., Messerschmidt, E., and Mulzer, D., "Steady State MPD Devices for Reentry Simulation," IEPC-88-114, *20th International Electric Propulsion Conference*, Garmisch-Partenkirchen, W. Germany, Oct. 1988.

[23]Winter, M., Auweter-Kurtz, M., Heiermann, J., and Wegmann, T., "Experimental and Numerical Comparison of High Power Steadys State MPD Thrusters with Radiation- and Water-Cooled Anodes," IEPC-2003-207, *28th International Electric Propulsion Conference*, Toulouse, France, Mar. 2003.

[24]Zuin, M., Antoni, V., Paganucci, F., Cavazzana, R., Serianna, G., Spolaore, M., Vianello, N., Bagatin, M., Rossetti, P., and Andrenucci, M., "Plasma Fluctuations in an MPD Thruster with and without the Application of an External Magnetic Field," IEPC-2003-299, *28th International Electric Propulsion Conference*, Toulouse, France, Mar. 2003.

[25]Paganucci, F., Rossetti, P., Andrenucci, M., Tikhonov, V., and Obukhov, V., "Performance of an Applied Field MPD Thruster with a Pre-Ionization Chamber," IEPC-2003-302, *28th International Electric Propulsion Conference*, Toulouse, France, Mar. 2003.

[26]Choueiri, E. and Zeimer, J., "Quasi-Steady Magnetoplasmadynamic Thruster Measured Performance Database," AIAA-98-3472, *34th AIAA/ASME/SAE/ASEE Joint Propulsion Conference,* Cleveland, OH, July 1998.

[27]Mikellides, P. G., Turchi, P. J., and Roderick, N. F., *J. Propulsion and Power*, **16** (5), Sep. 2000, pp. 887-893.

[28]Mikellides, P. G., and Turchi, P. J., *J. Propulsion and Power*, **16** (5), Sep. 2000. pp. 894-901.

[29]Diamant, K. D., Choueiri, E. Y., and Jahn, R. g., "The Role of Spot Mode Transition in the Anode Fall of Pulsed MPD Thrusters", IEPC-95-234, *24th International Electric Propulsion Conference*, Sept. 1995.

[30]Choueiri, E. Y., "MPD Thruster Plasma Instability Studies", AIAA-87-1067, *19th International Electric Propulsion Conference*, Colorado Springs, CO, May 1987,

[31]Choueiri, E. Y., Kelly, A. J., and Jahn, R. G., "Scaling of Thrust in Self-Field Magnetoplasmadynamic Thrusters", *J. Propulsion and Power*, **14** (5), Sep. 2000, pp. 744-753.

[32]Gilland, J. H. and Johnston, G., "MPD Thruster Performance Analytic Models", *Space Technologies and Applications International Forum 2003*, Albuquerque, NM, Feb. 2003.

[33]Gilland, J. H., Kelley, A. J., and Jahn, R. G., "MPD Thruster Scaling", AIAA-87-0997, *19th International Electric Propulsion Conference*, Colorado Springs, CO, May 1987.

34Auweter-Kurtz, M. and Messerschmid, E. W., "Plasma Accelerator Activities at the IRS", AIAA-90-2659, *21st International Electric Propulsion Conference*, Orlando, FL, July 1990.

REPORT DOCUMENTATION PAGE

Form Approved
OMB No. 0704-0188

Public reporting burden for this collection of information is estimated to average 1 hour per response, including the time for reviewing instructions, searching existing data sources, gathering and maintaining the data needed, and completing and reviewing the collection of information. Send comments regarding this burden estimate or any other aspect of this collection of information, including suggestions for reducing this burden, to Washington Headquarters Services, Directorate for Information Operations and Reports, 1215 Jefferson Davis Highway, Suite 1204, Arlington, VA 22202-4302, and to the Office of Management and Budget, Paperwork Reduction Project (0704-0188), Washington, DC 20503.

1. AGENCY USE ONLY (*Leave blank*)

2. REPORT DATE
September 2004

3. REPORT TYPE AND DATES COVERED
Technical Memorandum

4. TITLE AND SUBTITLE
High Power MPD Thruster Performance Measurements

5. FUNDING NUMBERS
WBS–22–319–20–E2

6. AUTHOR(S)
Michael R. LaPointe, Eugene Strzempkowski, and Eric Pencil

7. PERFORMING ORGANIZATION NAME(S) AND ADDRESS(ES)
National Aeronautics and Space Administration
John H. Glenn Research Center at Lewis Field
Cleveland, Ohio 44135–3191

8. PERFORMING ORGANIZATION REPORT NUMBER
E–14733

9. SPONSORING/MONITORING AGENCY NAME(S) AND ADDRESS(ES)
National Aeronautics and Space Administration
Washington, DC 20546–0001

10. SPONSORING/MONITORING AGENCY REPORT NUMBER
NASA TM—2004-213226
AIAA–2004–3467

11. SUPPLEMENTARY NOTES
Prepared for the 40th Joint Propulsion Conference and Exhibit cosponsored by AIAA, ASME, SAE, and ASEE, Fort Lauderdale, Florida, July 11-14, 2004. Michael R. LaPointe, Ohio Aerospace Institute, 22800 Cedar Point Road, Brook Park, Ohio 44142; Eugene Strzempkowski and Eric Pencil, NASA Glenn Research Center. Responsible person, Eric Pencil, organization code 5430, 216–977–7463.

12a. DISTRIBUTION/AVAILABILITY STATEMENT
Unclassified - Unlimited
Subject Category: 20 Distribution: Nonstandard
Available electronically at http://gltrs.grc.nasa.gov
This publication is available from the NASA Center for AeroSpace Information, 301–621–0390.

12b. DISTRIBUTION CODE

13. ABSTRACT ***(Maximum 200 words)***

High power magnetoplasmadynamic (MPD) thrusters are being developed as cost effective propulsion systems for cargo transport to lunar and Mars bases, crewed missions to Mars and the outer planets, and robotic deep space exploration missions. Electromagnetic MPD thrusters have demonstrated, at the laboratory level, the ability to process megawatts of electrical power while providing significantly higher thrust densities than electrostatic electric propulsion systems. The ability to generate higher thrust densities permits a reduction in the number of thrusters required to perform a given mission, and alleviates the system complexity associated with multiple thruster arrays. The specific impulse of an MPD thruster can be optimized to meet given mission requirements, from a few thousand seconds with heavier gas propellants up to 10,000 seconds with hydrogen propellant. In support of programs envisioned by the NASA Office of Exploration Systems, Glenn Research Center is developing and testing quasi-steady MW-class MPD thrusters as a prelude to steady-state high power thruster tests. This paper provides an overview of the GRC high power pulsed thruster test facility, and presents preliminary performance data for a quasi-steady baseline MPD thruster geometry.

14. SUBJECT TERMS
Propulsion; Electric propulsion; Electromagnetic propulsion; Plasma propulsion; Magnetoplasmadynamic thruster

15. NUMBER OF PAGES
19

16. PRICE CODE

17. SECURITY CLASSIFICATION OF REPORT	18. SECURITY CLASSIFICATION OF THIS PAGE	19. SECURITY CLASSIFICATION OF ABSTRACT	20. LIMITATION OF ABSTRACT
Unclassified	Unclassified	Unclassified	